IOP PUBLISHING JOURNAL OF PHYSICS: CONDENSED MATTER

J. Phys.: Condens. Matter **23** (2011) 374107 (9pp) doi:10.1088/0953-8984/23/37/374107

One-dimensional deterministic transport in neurons measured by dispersion-relation phase spectroscopy

Ru Wang[1], Zhuo Wang[2], Joe Leigh[2], Nahil Sobh[3], Larry Millet[4], Martha U Gillette[4], Alex J Levine[5] and Gabriel Popescu[2]

[1] Quantitative Light Imaging Laboratory, Department of Mechanical Science and Engineering, Beckman Institute for Advanced Science and Technology, University of Illinois at Urbana-Champaign, Urbana, IL 61801, USA
[2] Quantitative Light Imaging Laboratory, Department of Electrical and Computer Engineering, Beckman Institute for Advanced Science and Technology, University of Illinois at Urbana-Champaign, Urbana, IL 61801, USA
[3] Beckman Institute for Advanced Science and Technology, Department of Civil and Environmental Engineering, and Department of Mechanical Engineering and Sciences, University of Illinois at Urbana-Champaign, Urbana, IL 61801, USA
[4] Department of Cell and Developmental Biology, University of Illinois at Urbana-Champaign, Urbana, IL 61801, USA
[5] Department of Chemistry and Biochemistry and Department of Physics and Astronomy, University of California at Los Angeles, Los Angeles, CA 90095, USA

E-mail: alevine@chem.ucla.edu and gpopescu@illinois.edu

Received 22 February 2011, in final form 2 August 2011
Published 23 August 2011
Online at stacks.iop.org/JPhysCM/23/374107

Abstract
We studied the active transport of intracellular components along neuron processes using a new method developed in our laboratory: dispersion-relation phase spectroscopy. This method is able to quantitatively map spatially the heterogeneous dynamics of the concentration field of the cargos at submicron resolution without the need for tracking individual components. The results in terms of density correlation function reveal that the decay rate is linear in wavenumber, which is consistent with a narrow Lorentzian distribution of cargo velocity.

(Some figures in this article are in colour only in the electronic version)

1. Introduction

Cells rely on their ability to actively transport macromolecules and even organelles, since the passive diffusive transport of such low mobility objects would simply be too slow. This directed transport of intracellular components is particularly apparent during cell division, but is known to occur during all phases of the cell cycle [1]. The necessity of active transport is especially acute where intracellular cargos need to be carried over long distances, as in the case of the transport of intracellular vesicles and other large objects up and down the axonal and dendritic processes of neurons. In such narrow and elongated structures, the spatial distribution of these cellular transport highways is particularly simple: intracellular traffic is directed along an essentially one-dimensional, tortuous path in a three-dimensional space. This bidirectional (i.e. to and from the cell's soma) transport is known to be mediated by some combination of thermal diffusion and active stochastic transport driven by molecular motors (e.g. kinesin and dynein) [2–4], but these transport phenomena could be better understood through quantitative analysis. The reduction of complex transport networks commonly found in cell bodies to a one-dimensional system provides an opportunity for refining experimental techniques for transport measurement and theoretical modeling.

Using single molecule tracking, precise measurements of individual cargos that are transported by molecular motors have been made previously, see, e.g., [5]. In addition, the

motion of externally driven particles and the observation of their fluctuating position have been successfully used to monitor the viscoelastic properties of living cells [6, 7] and the 'active', or molecular motor-driven, strain fluctuations and cargo transport [8–10] in cytoskeletal networks. The fluctuations of one- and two-dimensional objects (e.g. filaments [1] and membranes [11]) have also been studied to measure the elastic properties and motor activity in living cells. In this paper we examine a complementary technique that does not require the tracking of individual particles and which investigates more globally the spatial and temporal nature of cargo transport over tens of microns and thousands of seconds. While we do not resolve the motion of individual cargos, we can quantitatively and spatially map the heterogeneous dynamics of the concentration field of the cargos with submicron resolution. Our method relies on quantifying interferometrically the path length map produced by cells [12].

Quantifying cell-induced shifts in the optical path-lengths permits nanometer scale measurements of structures and motions in a non-contact, non-invasive manner [13]. Thus, quantitative phase imaging (QPI) has recently become an active field of study and various experimental approaches have been proposed [14–23]. We have shown that the knowledge of the amplitude and phase associated with the image plane is equivalent to extremely sensitive elastic and quasi-elastic light scattering measurements [24–26]. This new approach represents the spatial equivalent of Fourier transform spectroscopy and is, thus, referred to as Fourier transform light scattering (FTLS). Recently, FTLS proved sensitive enough to quantify actin dynamics in unlabeled live cells [27].

Despite all these advances, the range of QPI applications in cellular biophysics has been largely limited to red blood cell imaging [11, 28–30] or assessment of global cell parameters such as dry mass [15, 31], average refractive index [32], and statistical parameters of tissue slices [25, 33]. This limitation is mainly due to the speckle generated by the high temporal coherence of the light used (typically lasers), which averages out the morphological details. Thus the contrast in QPI images has never matched that exhibited in white light techniques such as phase contrast and Nomarski.

Recently we developed SLIM (spatial light interference microscopy), a novel, highly sensitive QPI method, which promises to enable unprecedented structure and dynamics studies in biology and beyond [34]. SLIM reveals the intrinsic contrast of transparent samples like phase contrast microscopy [35], while rendering quantitative phase information, like holography [36]. Taken together, SLIM's features advance the field of quantitative phase imaging in several ways: (i) it provides speckle-free images, which allow for spatially sensitive optical path length measurement (0.3 nm); (ii) it uses common path interferometry, which enables temporally sensitive optical path length measurement (0.03 nm); (iii) it renders 3D tomographic images of transparent structures; (iv) due to the broad band illumination, SLIM grants immediate potential for spectroscopic (i.e. phase dispersion) imaging; (v) it is likely to make a broad impact by implementation with existing phase contrast microscopes; and (vi) it inherently multiplexes with fluorescence imaging for multimodal, in-depth biological studies.

The remainder of this paper is organized as follows: in section 2 we describe SLIM in more detail, focusing on its application to one-dimensional transport in neurites in section 3. In section 4 we discuss our analysis of the data in terms of simple advection diffusion models. We present the results of that analysis in section 5. Finally, we conclude with a discussion of the results and our interpretation thereof in section 6.

2. Spatial light interference microscopy (SLIM)

SLIM is described in more detail elsewhere [34]. In short, it is implemented as an extension to an existing phase contrast microscope that makes the instrument capable of quantifying phase shifts across the field of view. Both SLIM and phase contrast microscopy exploit the concept of imaging as an interference phenomenon, which was recognized more than a century ago by Abbe in the context of microscopy: 'the microscope image is the interference effect of a diffraction phenomenon' [37]. Describing an image as a (complicated) interferogram later set the basis for Gabor's development of holography [36].

Unlike the traditional phase contrast microscope, where a phase ring with a fixed phase shift of $\pi/2$ is introduced at the back focal plane of the phase contrast objective [37], in SLIM we map the back focal plane onto a phase-only spatial light modulator that introduces additional phase delays of 0, $\pi/2$, π, $3\pi/2$, as shown in figure 1(a). The Fourier lenses L_2 and L_1 form a 4f system, such that the spatially modulated image of the sample is recorded by the CCD. The phase shift distribution associated with the object, $\phi(\mathbf{r})$, can thus be retrieved from a combination of four phase shifted intensity images,

$$\phi(\mathbf{r}) = \arg\left[\frac{\beta(\mathbf{r})\sin[\Delta\phi(\mathbf{r})]}{1+\beta(\mathbf{r})\cos[\Delta\phi(\mathbf{r})]}\right]. \tag{1}$$

In equation (1), $\beta(\mathbf{r}) = |U_1(\mathbf{r})|/|U_0|$ is the ratio between the amplitudes of the scattered (U_1) and unscattered (U_0) fields; $\Delta\phi$ is the phase difference between the scattered and unscattered light, defined as

$$\Delta\phi(\mathbf{r}) = \arg\left[\frac{I(\mathbf{r};3\pi/2) - I(\mathbf{r};\pi/2)}{I(\mathbf{r};0) - I(\mathbf{r};\pi)}\right], \tag{2}$$

where $I(\mathbf{r};\delta)$ is the intensity image associated with each phase shift δ. Equations (1) and (2) show how the quantitative phase image is retrieved via four successive intensity images measured for each phase shift.

Compared with existing methods for quantitative phase imaging, SLIM benefits from a number of features, such as spatial sensitivity (0.3 nm) and temporal sensitivity (0.03 nm) in measuring optical path-lengths [34]. Since a minimal modification is brought to the existing phase contrast microscope, SLIM can also overlay with fluorescence imaging at the same time and render the high quality phase images as one channel for multimodal imaging.

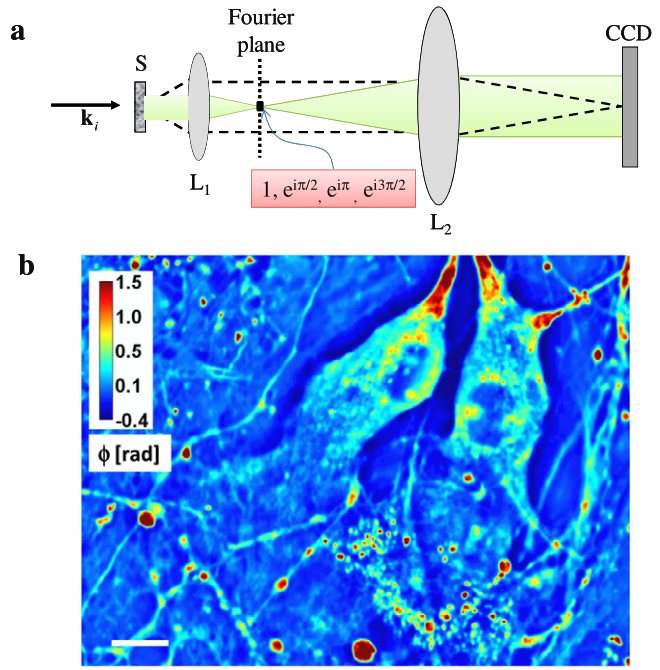

Figure 1. (a) The microscope as a scattering instrument: dashed line, scattered field; green (solid line), unscattered field; L_1, L_2, lenses; CCD, charged coupled device; $\mathbf{k_i}$, wavevector associated with the incident plane wave. (b) Quantitative phase images of live supraoptic magnocellular neurons in culture. The objective was 40×, 0.65NA for (b). The color bar indicates the phase in radians. Scale bar: 10 μm.

The ability of SLIM to render quantitative phase images of live, unlabeled cells is shown in figure 1(b). Due to the white light illumination, which alleviates the detrimental effects of speckle, SLIM reveals the structure of the cell in great detail. The measured path length fluctuations report on the dry mass transport within the cell [31]. Since most neuronal processes exhibit microtubule-mediated transport along their elongated structures, we can assume 1D dry mass density fluctuations, i.e., mass transport along the neurite, $\rho(s) \propto \Delta n(s)$, with $s = \sqrt{x^2 + y^2}$. From the time-lapse data, the microtubule-mediated transport along these neurites can be observed very clearly. However, the quantitative analysis of mass transport in these 1D structures is difficult due to their nonlinear shape. Therefore, first we numerically processed the images to 'straighten' the neurites, as described in section 3.

3. Image processing for studying 1D transport

For image processing, we used ImageJ, a Java-based program developed at the National Institutes of Health [38]. This platform allows the implementation of a plugin, referred to as NeuronJ, which was originally developed by Meijering *et al* to numerically trace neurites in fluorescence images [39]. We used this algorithm for SLIM images to delineate and segment neurites of arbitrary trajectories. Further, we used a cubic-spline interpolation method to straighten the neurites from a 2D path, $s = \sqrt{x^2 + y^2}$, to a 1D trajectory. This computational tool was developed by Kocsis *et al* in the context of electron microscopy (for more details, see [39]). Figures 2 and 3 illustrate how the path length information along individual neurites is extracted and represented along single lines. This numerical procedure was repeated for all the frames in the time-resolved data. The resulting x–t phase images were analyzed in terms of the dispersion relation, as detailed below.

4. Dispersion-relation phase spectroscopy (DPS)

The data from the phase images of many neurities are combined to compute the two-point correlation function of the mass density fluctuations $\rho(x, t)$ (assumed to be proportional to the fluctuations in the local index of refraction) in them:

$$g(x, \tau) = \langle \rho(x' + x, t + \tau)\rho(x', t)\rangle_{x',t}, \tag{3}$$

where the angled brackets here denote a spatial and temporal average. The observed temporal decay of this correlation function allows us to interpret the experimental data in terms of the stochastic dynamics of mass transport in the system. Fourier transforming the data,

$$\tilde{g}(q, \tau) = \int \mathrm{d}x\, g(x, \tau)\mathrm{e}^{-\mathrm{i}qx}, \tag{4}$$

we find that the decay of $\tilde{g}(q, \tau)$ is well fitted by a single exponential so that we can determine the q-dependence of that rate constant $\Gamma(q)$, characterizing stochastic dynamics on length scales of $\ell = 2\pi/q$. Representative examples of these extracted decay rates are shown in figure 3 as a function of wavenumber q.

The decay of correlations reflects the net effect of the motion of the material having various indices of refraction and velocities. We cannot distinguish *a priori* the independent contributions to the signal coming from various equilibrium (e.g. diffusion) and non-equilibrium processes such as the molecular motor-driven motion of vesicles or the dynamics of polymerization and depolymerization of, e.g., microtubules. Examining the data—see figure 2 ((d)–(g))—one notes that the observable dynamic heterogeneities appear to be localized or point-like objects, consistent with vesicles or groups of vesicles moving within the neurites. For brevity we refer to the mass transport dynamics generating the decay of correlations as 'vesicle motion' hereafter, although this cannot be concluded from the phase images alone. Independently of the ultimate identification of these mobile structures, we propose to characterize their dynamics in terms of an advection diffusion model in one dimension,

$$D\nabla^2\rho(x, t) - v\nabla\rho(x, t) - \frac{\partial}{\partial t}\rho(x, t) = 0, \tag{5}$$

describing the dynamics of the mass density field in terms of the combination of diffusion with the collective diffusion constant D and advection or active transport with speed v. We note that the effective diffusion constant is not expected to coincide with the equilibrium one as active stochastic active transport processes contribute to the effective diffusion of mass density in the system. We then assume that the observed decay of correlations results from the incoherent motion of many compact bodies having a distribution of advection

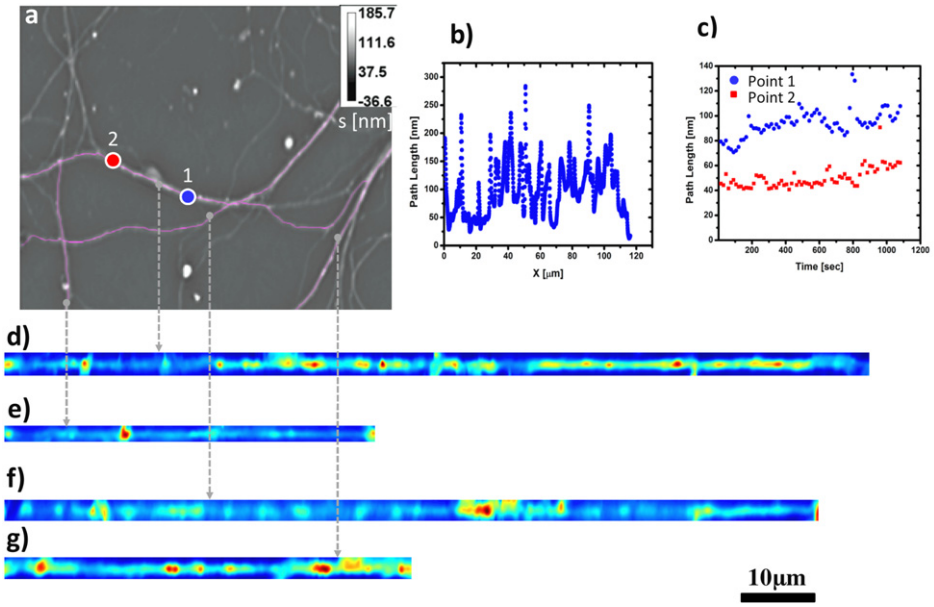

Figure 2. (a) Phase image of a neuron at 40× with a frame rate of about 15 s/frame to determine mass transport in neurites, labeled with a pink highlighted line. (b) Path length static distribution along an individual neurite (d). (c) Path length dynamic fluctuations over time at two locations (labeled blue circle (point1) and red square (point2)) of a neurite (d); (d)–(g) neurites of image (a) were traced and straightened with ImageJ plugins—NeuronJ and Straighten.

speeds $P(v)$. We discuss the suitability of these assumptions below.

There is a long history of studying transport in one-dimensional (1D) or nearly (to be defined below) 1D structures, which has implications for any analysis of mass transport in neurites. The long length scale properties of 1D transport are strongly influenced by two features. First the effect of steric interactions between the moving elements can be significant, an effect commonly encountered in traffic jams [40]. Alexander and Pincus showed that the non-driven or equilibrium dynamics of particles on a 1D track is actually subdiffusive, due to such steric effects [41]. The dynamics of the transport system of current interest is, however, expected to be dominated by the non-equilibrium advective effects of molecular motors at long length scales. Two classes of models have been studied that generate such steady-state currents, i.e. net mass transport that is distinguished by how the left/right symmetry of the problem is broken in order to generate such currents. In the first class the symmetry breaking term is introduced via boundary conditions by attaching the 1D track to a particle source and sink on opposite sides, as done in, e.g., [52]. In the second class one postulates a nonzero mean force acting on the particles. We expect this latter class of models to be appropriate for the system of current interest since it is known that molecular motors actively transport cargos in fixed directions relative to polarized tracks within neurites [40, 42]. More generally, both inherently symmetric models driven by boundary conditions, known as symmetric exclusion processes (SEP), and symmetry breaking systems or asymmetric exclusion processes (ASEP) have been explored in a variety of contexts including models of proton transfer in water channels [43], mRNA translation [44], in addition to the problem under consideration, the motion of cargos driven by molecular motors along microtubules [40, 42, 45]. The more idealized system of perfectly unidirectional stochastic motion (i.e. no backwards steps allowed) motion, known as totally asymmetric exclusion processes (TASEP), has also generated intense interest in part from its role as a tractable model system with which to explore nontrivial non-equilibrium steady states [46].

Our approach to the dynamics is in the spirit of various hydrodynamic approximations to the ASEP models used to treat the long wavelength and low frequency dynamics of such systems. These models, often including binding/unbinding or Langmuir kinetics in addition to the 1D motion, result in complex dynamics for the particle density field [47–49]. These dynamics can be described by a Burgers equation for the density field, which is well known to exhibit moving shock fronts [47] or rapid jumps in particle density. Of course, transport in the neurite takes place along a bundle of 1D tracks with driven transport in both directions. Such generalizations having multiple tracks [50, 51] have been explored for both ASEP [52–54] and SEP systems.

Our analysis of the dynamics as the sum of a variety of independent advection/diffusion processes neglects large correlated motions resulting from the excluded volume interaction. We believe that this linearized model is a reasonable starting point for data analysis for two reasons. There is evidence that multiple tracks or allowance for slippage of cargos past each other (i.e. 'nearly 1D models') minimizes the role of large correlated motions [52]. In the presence of such strong interactions, however, we expect the collective excitations of the particle density (e.g. Burgers shocks) to move roughly independently so that, even in the case of strong correlations in the density of moving particles,

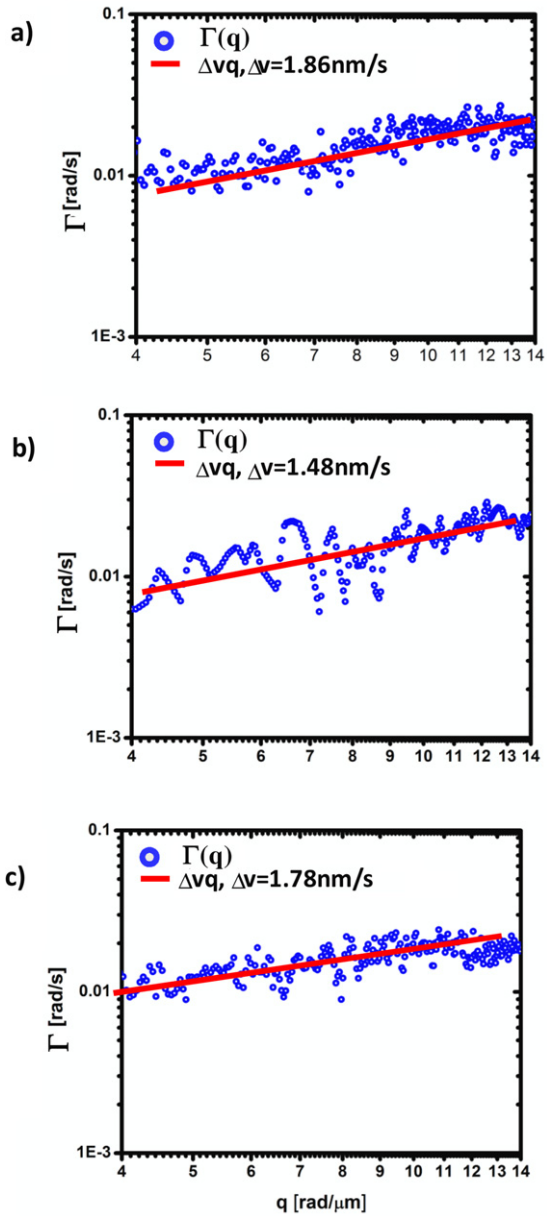

Figure 3. (a)–(c) Dispersion-relation curves (blue) for straightened neurites (d)–(f) of figure 2. The solid lines indicate the linear fit. The fit parameter, Δv, represents the bandwidth of the directed motion speed distribution.

the index of refraction changes, to which we are sensitive, should reflect the dynamics of weakly interacting collective phenomena when viewed at long length scales.

Returning to our advection diffusion model, we determine from equation (5) the temporal decay of the autocorrelation function of the mass density $\tilde{g}$ (defined by equations (3) and (4)). It is straightforward to show that at wavenumber q, this function takes the form

$$\tilde{g}(q,\tau) = g_0 \mathrm{e}^{[\mathrm{i}qv - Dq^2]\tau}. \tag{6}$$

Equation (6) relates the measured temporal autocorrelation function to the diffusion coefficient, D, and advection velocity, v, of the matter in the system. The experimental data, however, reflect the net effect of the motion of many vesicles, each having its own local transport velocity depending on, e.g., the size of the vesicle and the number of molecular motors attached to it. The observed autocorrelation function then should be the sum or average over a broad distribution of advection velocities $P(v)$. The advection-velocity-averaged autocorrelation function is proportional to the Fourier transform of the advection velocity distribution

$$[\tilde{g}(q,\tau)]_P = g_0 \mathrm{e}^{-Dq^2\tau} \int \mathrm{d}v\, P(v) \mathrm{e}^{\mathrm{i}vq\tau}, \tag{7}$$

where the square brackets $[\bullet]_P$ denote an average over the distribution of advection velocities $P(v)$. This distribution remains to be determined. The integral in equation (7) is the moment generating function of $P(v)$ with $\mathrm{i}q\tau$ as the independent variable. Thus the natural logarithm of equation (7),

$$\ln([\tilde{g}(q,\tau)]_P) = \ln g_0 - \tau \left\{ Dq^2 - \frac{1}{\tau} K(\mathrm{i}q\tau) \right\}, \tag{8}$$

can be written in terms of the cumulant generating function $K(x) = \ln \int \mathrm{d}v\, P(v) \mathrm{e}^{\mathrm{i}xv}$. For any distribution having a finite second moment we find from equation (8) that

$$\ln([\tilde{g}(q,\tau)]_P) = \ln g_0 - \tau D q^2 - \mathrm{i}q\tau \langle v \rangle - \tfrac{1}{2} q^2 \tau^2 [\langle v^2 \rangle - \langle v \rangle^2] + \cdots, \tag{9}$$

where the higher order terms are proportional to the product of the nth cumulant of the advection velocity distribution and $(q\tau)^n$. Examining equation (9) we note that the dominant terms controlling the time evolution of the correlation function at small wavenumber consist of an oscillatory term linear in q and proportional to the mean advection velocity plus a term quadratic in q that depends on a combination of the diffusion constant D and the variance of the advection velocity distribution. Comparing this result with our data, we observe two things. First, this result is not consistent with the observed decay rate that is linear in wavenumber q and does not exhibit oscillations. Second, we do not observe a term proportional to τ^2. We conclude that the mean velocity must be sufficiently small that the oscillatory contribution to the correlation function is a frequency so low as to be not observable over the time of observation. This is not surprising in that we expect to observe the net effect of mass transport along both directions in each neurite. Such bidirectional transport is in itself not surprising. Since there is little or no net transport of mass down these structures over the period of observation, the observed mean velocity should vanish. Moreover, we note that the advection velocity distribution must be sufficiently broad to have a divergent second moment.

Based on this analysis we attempt to fit the data by choosing a Lorentzian distribution with width Δv and small but nonzero mean $\langle v \rangle_v \neq 0$. This leads, by direct integration of equation (7), to a linear dependence of the decay rate on wavenumber

$$[\tilde{g}(q,\tau)]_P = \mathrm{e}^{-Dq^2\tau} \mathrm{e}^{\mathrm{i}\langle v \rangle q\tau - \Delta v |q\tau|}. \tag{10}$$

Of course it is not possible for the distribution of motor velocities to be truly Lorentzian since the motors' maximal

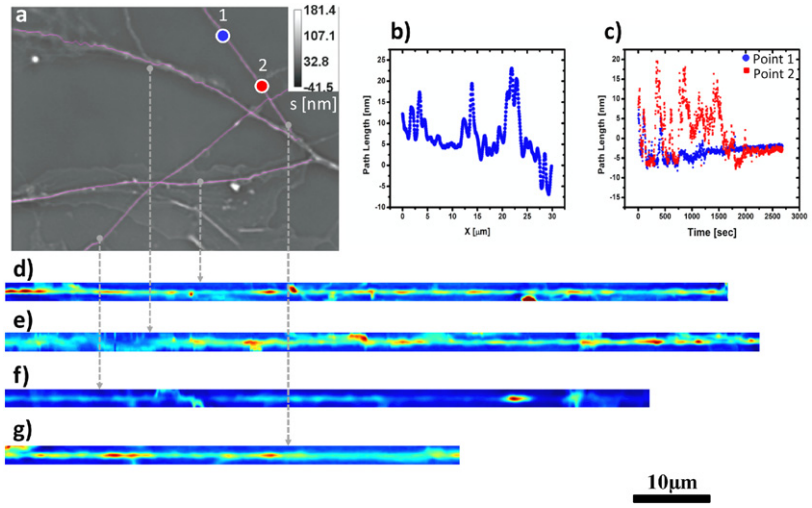

Figure 4. (a) Phase image of mass transport in neurites of hippocampal neurons. The image was acquired at 63× with a frame rate of 2 s/frame, the pink highlighted lines represent the data subsets analyzed in (b)–(g). (b) Path length static distribution along an individual neurite (g). (c) Path length dynamic fluctuations over time at two locations (labeled blue circle (point1) and red square (point2)) of a neurite (d); (d)–(g) neurites of image (a) were traced and straightened with ImageJ plugins—NeuronJ and Straighten.

speed is finite. For kinesin motors, this maximum is known to be approximately $v_{\max} = 0.8\ \mu\text{m s}^{-1}$ [55]. Accordingly, we take a $P(v)$ to be Lorentzian with both a mean v_{m} and width Δv much smaller than the cutoff velocity, v_{m}, $\Delta v \ll v_{\max}$:

$$P(v) = \frac{P_0}{(v - v_{\text{m}})^2 + \Delta v^2}\Theta(v_{\max} - |v|), \tag{11}$$

where $\Theta(x)$ is the Heaviside step function and the normalization constant $P_0 \approx \Delta v/2 \arctan(v_{\max}/\Delta v)$ for a small mean velocity. The normalization is exact in the limit that $v_{\text{m}} = 0$. Since we expect to observe transport in both directions with essentially equal probability, we expect the mean advection speed to be significantly lower than the maximum motor speed. Of course the assumption that both the width and mean of the advection velocity distribution are small compared to the maximum velocity can be checked *a posteriori*.

Applying this cutoff Lorentzian model to the integral in equation (10) one can show that

$$\tilde{g}(q,\tau) \approx g_0 \mathrm{e}^{\mathrm{i}q\tau v_{\text{m}} - Dq^2\tau}\mathrm{e}^{-q\tau\Delta v}\left[1 + \frac{2\Delta v \mathrm{e}^{q\tau\Delta v}\cos(v_{\max}q\tau)}{\pi v_{\max}} + \frac{2q\tau\Delta v \mathrm{e}^{q\tau\Delta v}}{\pi}\left(\mathrm{Si}(v_{\max}q\tau) - \frac{\pi}{2}\right)\right], \tag{12}$$

where $\mathrm{Si}(x)$ is the sine integral. The final term in the product may be neglected in the limit that $\Delta v/v_{\max} \ll 1$ and $v_{\max}q\tau \gg 1$, both of which are valid for the data in question. Thus, the effect of the large velocity cutoff is subdominant and the wavenumber dependent decay rate of the autocorrelation function is a sum of linear and quadratic terms in q, representing the effects of motor-generated advection and diffusion, respectively. We may write this decay rate as

$$\Gamma(q) = \Delta v q + Dq^2. \tag{13}$$

This relationship between the decay rate Γ and its wavenumber q represents the dispersion relationship associated with intracellular transport and provides insight into the diffusion coefficient and velocity distribution. We refer to this method as dispersion-relation phase spectroscopy (DPS).

5. Results

We applied DPS to various neuronal structures in different cultures and over a broad range of temporal and spatial scales. Figure 2 summarizes the results obtained by imaging a field of neurites for 18 min at a rate of 1 frame per 15 s. A quantitative phase map measured by SLIM is shown in figure 2(a), where the grayscale bar indicates the path length in nanometers and the neuritic structures of interest are highlighted. Figure 2(b) exemplifies the path length fluctuation around a single neurite and indicates the highly inhomogeneous nature of the neurite's structure. Further, this signal, which is, up to a constant, the mass density, $\rho(x)$, is characterized by high signal to noise, which translates into high spatial sensitivity to density fluctuations. Temporally, the density fluctuations associated with two arbitrary points are shown in figure 2(c). These signals show that SLIM can detect nanometer scale path length changes, which translate into minute changes in local mass density.

We applied the algorithm described in section 3 to numerically 'straighten' the neurites (figure 2(d)–(g)) such that the 1D diffusion–advection equation can be employed in a straightforward manner. For each neurite, the x–t data were Fourier transformed both spatially and temporally and the decay rate, $\Gamma(q)$, was retrieved. Remarkably, as shown in figure 3, all the $\Gamma(q)$ plots exhibit linear behavior, which is consistent with a signal resulting from a broad distribution of advection velocities. It is not consistent with an advection velocity distribution that has a finite second moment. We do not observe a signal consistent with diffusive transport. This is reasonable since it is known that diffusion

is not an efficient mechanism for this type of long-range transport associated with neurites [56] compared to active or motor-driven mass transport. Interestingly, we found that the bandwidths of the speed distributions for the three neurites, $\Delta v = 1.86, 1.48, 1.78$ nm s^{-1}, are very close in value, which may indicate a universal mechanism for this directed stochastic motion.

In order to confirm these findings on a different cell culture, with different imaging resolution and acquisition rates, we applied DPS to a neurite system where the acquisition rate was 7.5 times faster and the spatial resolution was higher by a factor of 2 (figure 4). The analysis procedure is analogous to that shown in figures 2 and 3. Notably, the results of these measurements at different spatio-temporal resolutions match closely those obtained before. Thus, for all neurites the results indicate deterministic transport, as shown in figure 5. The speed bandwidth values, $\Delta v = 2.08, 3.94, 1.92$ nm s^{-1}, are somewhat higher that in the previous case, but still in the same range. This similarity in the measured values suggests a commonality of transport mechanisms in the dendritic arbor of neurons.

The mean advection velocity extracted from the data is consistent with zero. From the resolution limit ($\approx$1 μm) and observation time ($\approx$1000 s), we may set an upper limit on the net drift velocity of 1 nm s^{-1}. We do not observe net mass transport down the neurites. Finally, we note that the assumptions made in the use of the cutoff Lorentzian appear to be justified.

6. Summary and discussion

We have found that the autocorrelation function in neurites is inconsistent with purely passive diffusive motion of cargos, but can be interpreted using a simple model of advective transport in which individual cargos are moved in both directions and with a Lorentzian range of speeds having nearly zero mean (due to equal rates of mass transport toward and away from the cell's soma) and a fairly narrow distribution about that vanishing mean, at least compared with the maximum velocity associated with active motors. This result is puzzling in that, given the extracted distribution of advection velocities, one cannot expect to observe cargos transported at speeds comparable to the reported maximum motor velocities. We may speculate as to the cause of the absence of fast movers. Assuming that the observed mass transport reflects the motion of individual motors, there are two possible interpretations of this result. First, the motors may, in fact, be operating near the stall force, where mean velocities are low and velocity fluctuations become significant. This proposed scenario seems to be physiologically inefficient and therefore unlikely. Alternatively, the motors are operating at forces where cargo detachment becomes frequent. If the cargos detach from the motors sufficiently frequently in the crowded viscoelastic environment of the neurites then, although the motors are still moving rapidly, the fraction of the time in which the cargos are being actively transported is small and consequently their observed advection speeds may be much smaller than

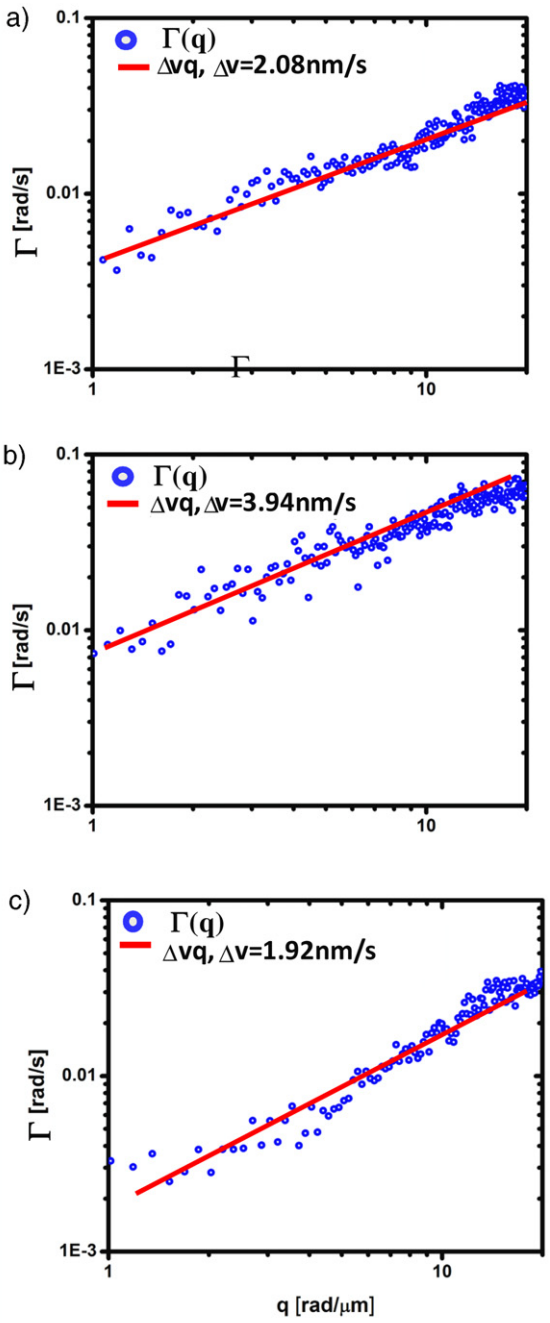

Figure 5. (a)–(c) Dispersion-relation curves (circles) for straightened neurites (d)–(f) of figure 4. Note the broad q-coverage due to the high NA objective. The solid lines indicate the linear fit. The fit parameter, Δv, represents the bandwidth of directed motion speed distribution.

those of the motors. Finally, it is possible that the mass transport to which we are sensitive reflects slow collective motions of many cargos, e.g. shock fronts in the density field, that may not move with the same velocity as the underlying motor-driven cargos. This appears to be the most reasonable explanation since it is known that the shock fronts can be significantly slower than the transport speeds of the individual cargos [57]. Clearly, simultaneous tracking of the cargos, motors, and mass density is necessary resolve this

issue. Similarly, theoretical advances are necessary to better understand the collective behavior of the mass density field in multi-track driven systems with steric interactions. We note that our result, i.e. the linear in wavenumber decay rate of the autocorrelation function, is not consistent with a velocity distribution that decays sufficiently rapidly at large velocities to have a finite second moment. The proposed Lorentzian, albeit with a narrow width compared to the maximum motor velocity, reflects a broad probability distribution.

Acknowledgments

AJL thanks A Carlsson for helpful conversations regarding the data analysis and thanks T Chou and E Frey for enjoyable conversations and for communicating unpublished work on ASEP problems. GP acknowledges support from the National Science Foundation (CBET 08-546660 CAREER, CBET-1040462 MRI) and National Cancer Institute (R21 CA147967-01). AJL acknowledges support from NSF-DMR-0907212. MUG and GP are supported by the NSF-STC CBET-0939511. MUG is supported by NIH grants HL 086870 and MH 085220. Additional support was provided by NSF CHE-0526692 (to MUG). LM was supported by NIH/HD007333 Developmental Psychobiology and Neurobiology Training Grant. JL, NS and GP acknowledge tool development support from the NSF Network for Computational Nanotechnology.

References

[1] Vallee R B and Sheetz M P 1996 Targeting of motor proteins *Science* **271** 1539–44
[2] MacKintosh F C and Schmidt C F 2010 Active cellular materials *Curr. Opin. Cell Biol.* **22** 29–35
[3] Brangwynne C P, Koenderink G H, MacKintosh F C and Weitz D A 2008 Cytoplasmic diffusion: molecular motors mix it up *J. Cell Biol.* **183** 583–7
[4] Brangwynne C P, Koenderink G H, MacKintosh F C and Weitz D A 2009 Intracellular transport by active diffusion *Trends Cell Biol.* **19** 423–7
[5] Yildiz A, Forkey J N, McKinney S A, Ha T, Goldman Y E and Selvin P R 2003 Myosin V walks hand- over-hand: single fluorophore imaging with 1.5 nm localization *Science* **300** 2061–5
[6] Trepat X, Deng L H, An S S, Navajas D, Tschumperlin D J, Gerthoffer W T, Butler J P and Fredberg J J 2007 Universal physical responses to stretch in the living cell *Nature* **447** 592
[7] Fabry B, Maksym G N, Butler J P, Glogauer M, Navajas D and Fredberg J J 2001 Scaling the microrheology of living cells *Phys. Rev. Lett.* **8714** 148102
[8] Caspi A, Granek R and Elbaum M 2000 Enhanced diffusion in active intracellular transport *Phys. Rev. Lett.* **85** 5655–8
[9] Mizuno D, Tardin C, Schmidt C F and MacKintosh F C 2007 Nonequilibrium mechanics of active cytoskeletal networks *Science* **315** 370–3
[10] Wang B, Anthony S M, Bae S C and Granick S 2009 Anomalous yet Brownian *Proc. Natl Acad. Sci. USA* **106** 15160–4
[11] Park Y K, Best C A, Badizadegan K, Dasari R R, Feld M S, Kuriabova T, Henle M L, Levine A J and Popescu G 2010 Measurement of red blood cell mechanics during morphological changes *Proc. Natl Acad. Sci. USA* **107** 6731
[12] Popescu G 2008 *Methods in Cell Biology* ed B P Jena (San Diego, CA: Academic) 87–115
[13] Popescu G 2008 *Methods in Cell Biology* vol 87, ed P J Bhanu (Amsterdam: Elsevier)
[14] Paganin D and Nugent K A 1998 Noninterferometric phase imaging with partially coherent light *Phys. Rev. Lett.* **80** 2586–9
[15] Zicha D and Dunn G A 1995 An image-processing system for cell behavior studies in subconfluent cultures *J. Microsc.* **179** 11–21
[16] Yang C H, Wax A, Dasari R R and Feld M S 2001 Phase-dispersion optical tomography *Opt. Lett.* **26** 686–8
[17] Choma M A, Ellerbee A K, Yang C H, Creazzo T L and Izatt J A 2005 Spectral-domain phase microscopy *Opt. Lett.* **30** 1162–4
[18] Fang-Yen C, Oh S, Park Y, Choi W, Song S, Seung H S, Dasari R R and Feld M S 2007 Imaging voltage-dependent cell motions with heterodyne Mach–Zehnder phase microscopy *Opt. Lett.* **32** 1572–4
[19] Joo C, Akkin T, Cense B, Park B H and de Boer J E 2005 Spectral-domain optical coherence phase microscopy for quantitative phase-contrast imaging *Opt. Lett.* **30** 2131–3
[20] Rockward W S, Thomas A L, Zhao B and DiMarzio C A 2008 Quantitative phase measurements using optical quadrature microscopy *Appl. Opt.* **47** 1684–96
[21] Popescu G, Ikeda T, Dasari R R and Feld M S 2006 Diffraction phase microscopy for quantifying cell structure and dynamics *Opt. Lett.* **31** 775–7
[22] Ikeda T, Popescu G, Dasari R R and Feld M S 2005 Hilbert phase microscopy for investigating fast dynamics in transparent systems *Opt. Lett.* **30** 1165–8
[23] Popescu G, Deflores L P, Vaughan J C, Badizadegan K, Iwai H, Dasari R R and Feld M S 2004 Fourier phase microscopy for investigation of biological structures and dynamics *Opt. Lett.* **29** 2503–5
[24] Ding H F, Wang Z, Nguyen F T, Boppart S A, Millet L J, Gillette M U, Liu J M, Boppart M D and Popescu G 2010 Fourier transform light scattering (FTLS) of cells and tissues *J. Comput. Theor. Nanosci.* **7** 2501–11
[25] Ding H, Nguyen F, Boppart S A and Popescu G 2009 Optical properties of tissues quantified by Fourier transform light scattering *Opt. Lett.* **34** 1372
[26] Ding H F, Wang Z, Nguyen F, Boppart S A and Popescu G 2008 Fourier transform light scattering of inhomogeneous and dynamic structures *Phys. Rev. Lett.* **101** 238102
[27] Ding H, Millet L J, Gillette M U and Popescu G 2010 Actin-driven cell dynamics probed by Fourier transform light scattering *Biomed. Opt. Express* **1** 260
[28] Popescu G, Ikeda T, Goda K, Best-Popescu C A, Laposata M, Manley S, Dasari R R, Badizadegan K and Feld M S 2006 Optical measurement of cell membrane tension *Phys. Rev. Lett.* **97** 218101
[29] Park Y K, Diez-Silva M, Popescu G, Lykotrafitis G, Choi W, Feld M S and Suresh S 2008 Refractive index maps and membrane dynamics of human red blood cells parasitized by plasmodium falciparum *Proc. Natl Acad. Sci. USA* **105** 13730
[30] Park Y K, Best C A, Auth T, Gov N, Safran S A, Popescu G, Suresh S and Feld M S 2010 Metabolic remodeling of the human red blood cell membran *Proc. Natl Acad. Sci. USA* **107** 1289
[31] Popescu G, Park Y, Lue N, Best-Popescu C, Deflores L, Dasari R R, Feld M S and Badizadegan K 2008 Optical imaging of cell mass and growth dynamics *Am. J. Physiol. Cell Physiol.* **295** C538–44
[32] Lue N, Popescu G, Ikeda T, Dasari R R, Badizadegan K and Feld M S 2006 Live cell refractometry using microfluidic devices *Opt. Lett.* **31** 2759

[33] Ding H, Wang Z, Nguyen F, Boppart S A and Popescu G 2008 Fourier transform light scattering of inhomogeneous and dynamic structures *Phys. Rev. Lett.* **101** 238102
[34] Wang Z, Millet L J, Mir M, Ding H, Unarunotai S, Rogers J A, Gillette M U and Popescu G 2011 Spatial light interference microscopy (SLIM) *Opt. Express* **19** 1016
[35] Zernike F 1955 How I discovered phase contrast *Science* **121** 345
[36] Gabor D 1948 A new microscopic principle *Nature* **161** 777
[37] Zernike F 1942 Phase contrast, a new method for the microscopic observation of transparent objects, part 1 *Physica* **9** 686–98
[38] Rasband W S 1997–2009 *ImageJ* US National Institutes of Health, Bethesda, Maryland, USA http://rsb.info.nih.gov/ij/
[39] Meijering E, Jacob M, Sarria J C F, Steiner P, Hirling H and Unser M 2004 Design and validation of a tool for neurite tracing and analysis in fluorescence microscopy images *Cytometry* A **58A** 167–76
[40] Chowdhury D, Schadschneider A and Nishinari K 2005 Physics of transport and traffic phenomena in biology: from molecular motors and cells to organisms *Phys. Life Rev.* **2** 318–52
[41] Alexander S and Pincus P 1978 Diffusion of labeled particles on one-dimensional chains *Phys. Rev.* B **18** 2011–2
[42] Chowdhury D, Basu A, Garai A, Greulich P, Nishinari K, Schadschneider A and Tripathi T 2008 Intra-cellular traffic: bio-molecular motors on filamentary tracks *Eur. Phys. J.* B **64** 593–600
[43] Chou T 2004 Water alignment, dipolar interactions, and multiple proton occupancy during water-wire proton transport *Biophys. J.* **86** 2827–36
[44] Shaw S L, Kamyar R and Ehrhardt D W 2003 Sustained microtubule treadmilling in Arabidopsis cortical arrays *Science* **300** 1715–8
[45] Pierobon P 2009 Traffic of molecular motors: from theory to experiments *Traffic and Granular Flow'07* 679–88
[46] Spitzer F 1970 Interaction of Markov processes *Adv. Math.* **5** 246–90
[47] Evans M R, Juhasz R and Santen L 2003 Shock formation in an exclusion process with creation and annihilation *Phys. Rev.* E **68** 026117
[48] Parmeggiani A, Franosch T and Frey E 2003 Phase coexistence in driven one-dimensional transport *Phys. Rev. Lett.* **90** 086601
[49] Parmeggiani A, Franosch T and Frey E 2004 Totally asymmetric simple exclusion process with Langmuir kinetics *Phys. Rev.* E **70** 046101
[50] Kim K H and den Nijs M 2007 Dynamic screening in a two-species asymmetric exclusion process *Phys. Rev.* E **76** 021107
[51] Wood A J 2009 A totally asymmetric exclusion process with stochastically mediated entrance and exit *J. Phys. A: Math. Theor.* **42** 045002
[52] Chou T 1999 Kinetics and thermodynamics across single-file pores: solute permeability and rectified osmosis *J. Chem. Phys.* **110** 606–15
[53] Kolomeisky A B 1997 Exact solutions for a partially asymmetric exclusion model with two species *Physica* A **245** 523–33
[54] Pronina E and Kolomeisky A B 2004 Two-channel totally asymmetric simple exclusion processes *J. Phys. A: Math. Gen.* **37** 9907–18
[55] Coy D L, Wagenbach M and Howard J 1999 Kinesin takes one 8 nm step for each ATP that it hydrolyzes *J. Biol. Chem.* **274** 3667–71
[56] Wang R, Wang Z, Millet L, Gillette M U, Levine A J and Popescu G 2011 Dispersion-relation phase spectroscopy of intracellular transport *Opt. Exp.* under review
[57] Frey E 2011 personal communication